Contents lists available at SciOpen

Food Science and Human Wellness

journal homepage: https://www.sciopen.com/journal/2097-0765

China Food Publishing Co.

Salidroside alleviates ferroptosis of retinal ganglion cells in *db/db* mice

Wenqiang Liu[a,b], Anqi Liu[a], Yufei Wang[a], Shengxue Yu[b], Chuang Feng[a], Wanpeng Liu[b], Yan Fang[a], Jing Li[b], Hongdan Yu[b], Jiayou Liu[b], Wenjuan Wang[b], Jiayuan Ding[a], Pan Lü[c], Lipan Zhao[c], Linqin Luo[d], Xuezheng Liu[a,b,*], Zhongfu Zuo[a,b,*]

[a] *Department of Anatomy, School of Basic Medicine, Jinzhou Medical University, Jinzhou 121001, China*
[b] *Liaoning Key Laboratory of Diabetic Cognitive and Perceptive Dysfunction, Jinzhou Medical University, Jinzhou 121001, China*
[c] *Tianjin Medical University Cancer Institute and Hospital, National Clinical Research Center for Cancer, Tianjin 300202, China*
[d] *Xi'an Jiaotong University Health Science Center, Xi'an 710061, China*

ARTICLE INFO

Article history:
Received 18 January 2024
Received in revised form 14 February 2024
Accepted 1 July 2024

Keywords:
Diabetic retinopathy
Retinal ganglion cells
Ferroptosis
Salidroside

ABSTRACT

Salidroside (Sal), is one of the important food supplements from the traditional Chinese medicine *Integripetal rhodiola* herb, encapsulating significant anti-oxidative stress, anti-ferroptosis, and neuroprotective attributes. Notwithstanding these latent virtues, the ramifications of Sal on retinal ganglion cells (RGCs) impairment during the incipient stages of diabetic retinopathy (DR) remain equivocal. The purpose of this study was to investigate inhibitory effect of Sal on ferroptosis of RGCs in *db/db* mice. Within the research conducted, Sal was administered *via* gavage, and observations were made 8 weeks post-treatment. Retinal samples were collected for analysis. The results evidenced that Sal ameliorated blood glucose levels, attenuated RGCs destruction, and augmented visual functionality in *db/db* mice. Additionally, Sal exerted an anti-ferroptosis impact on the RGCs in the *db/db* mice. Successive discoveries have outlined the involvement of the HIF-1α/HO-1 signaling pathway in this protective mechanism. Ferroptosis of RGCs has a contributory effect on the development of DR, in part through the HIF-1α/HO-1 pathway. Intriguingly, Sal reversed the alterations in the HIF-1α/HO-1 pathway in *db/db* mice and displayed prospective advantageous effects on DR. Sal mitigated RGCs ferroptosis by reducing blood sugar and impeding the HIF-1α/HO-1 signaling pathway, thereby improving DR. Thus, Sal shows potential for use as a pharmaceutical and nutraceutical for DR.

1. Introduction

Diabetic retinopathy (DR) is a serious microvascular complication and a leading cause of vision loss or blindness among adults globally[1-2]. Hyperglycemia-elicited oxidative stress injury is discerned as a central pathogenic determinant in DR[3-4]. Retinal ganglion cells (RGCs), the exclusive neurons that convert optical energy into cellular membrane potential for transmission to the brain, are susceptible to oxidative harm, particularly within mitochondria-enriched RGCs axons, culminating in the demise of these metabolically dynamic cells[5-6]. Oxidative stress is instrumental in diverse RGCs death paradigms, encompassing apoptosis, necrosis, and autophagy[5,7-8]. However, interventions targeting these death paradigms afford merely fractional neuroprotection, intimating the plausible engagement of a discrete cell death paradigm in RGCs attrition.

Several molecular and cellular mechanisms contribute to RGCs injury in DR. These mechanisms encompass oxidative stress, mitochondrial dysfunction, inflammation, and glutamate neurotoxicity, all of which are associated with ferroptosis, a form of cell death characterized by lipid peroxidation and iron accumulation. Notably,

* Corresponding authors at: Department of Anatomy, School of Basic Medicine, Jinzhou Medical University, Jinzhou 121001, China.
E-mail address: liuxuezheng@jzmu.edu.cn (X.Z. Liu); zuozhongfu@jzmu.edu.cn (Z.F. Zuo)
Peer review under responsibility of Beijing Academy of Food Sciences.

SciOpen Publishing services by Tsinghua University Press

http://doi.org/10.26599/FSHW.2024.9250349

the buildup of iron has been observed in both type 1 and type 2 diabetic mouse models, as well as in the retinas of diabetic patients, exacerbating the progression of DR[9-10]. However, the precise role of RGCs ferroptosis in the development of DR remains unclear. Salidroside (Sal), is a compound extracted from *Rhodiola rosea* L. and serves as the primary active ingredient of this plant. Sal has multiple biological functions, including pronounced anti-oxidative stress, anti-ferroptosis, and neuroprotective capabilities, thus imparting protection against numerous ailments related to the nervous system and diabetes[11-13]. Recent studies have found that Sal can alleviate microvascular lesions in *db/db* mice by reducing oxidative stress[14]. Our research group also found that Sal can inhibit ganglion cell apoptosis by inhibiting the inflammatory response of Müller cells induced by streptozotocin (STZ)[15]. Salidroside can significantly improve the pyroptosis of RGC cells induced by diabetes[16]. Nevertheless, the potential prophylactic impact of Sal on RGCs ferroptosis in DR awaits clarification.

This inquiry authenticated the suppressive effect of Sal on ferroptosis in DR *db/db* mice RGCs and *in vitro*. At a molecular tier, bioinformatics and molecular docking procedures were deployed to prognosticate the action target of Sal, pinpointing hypoxia inducible factor-1 α (HIF-1α) as a plausible cardinal factor through which Sal bestows its protective influence. *In vitro* experiments utilizing HIF-1α inhibitors or activators further corroborated that Sal could mitigate RGCs ferroptosis by impeding the HIF-1α/HO-1 pathway. The observations not only proffer a novel perspective on the etiology of DR but also potential clinical prevention of DR and the cultivation of Sal as a therapeutic agent.

2. Materials and methods

2.1 Animals studies

All experimental steps got carried out in strict accordance with established principles aimed at minimizing both the quantity of animals used and the distress experienced by them. Protocol received endorsement from the Experimental Animal Ethics Committee of Jinzhou Medical University (No. 2022050801), and fully complied with the Guide for the Care and Use of Laboratory Animals (Permit Number: SYXK [Liao] 2019-0007). Male *db/db* mice ($BKS/DB^{-/-}$), aged 8 weeks, and their age-matched nondiabetic counterparts ($BKS/DB^{+/+}$, *db*/*m*) were obtained from Beijing Huafukang Biotechnology Co., Ltd. (Beijing, China). The diabetic mice had an average weight of (31 ± 2) g, while the nondiabetic littermates had an average weight of (20 ± 2) g. The specimens got accommodated in transparent plastic cages (n = 3 per cage), maintained at 22 ℃ constantly and subjected to a 12 h light-dark cycle (lights operational from 08:00 to 20:00). The mice were allowed free access to standard rodent chow and tap water without any restrictions during the duration of the study. Upon reaching the age of 12 weeks, the mice got randomly divided to 4 cohorts: vehicle-treated *db*/*m*, Sal-treated (Dalian Meilun Bio-Technology, Dalian, China; purity > 98%, MB6669, 100 mg/kg, once a day) *db*/*m*, vehicle-treated *db/db* mice, and Sal-treated (100 mg/kg, once a day) *db/db* group, 12 mice per group. Sal got prepared in a saline solution and administered to the mice *via* gavage for a period of 8 weeks. The *db*/*m* and *db/db* groups receiving the vehicle treatment were given an equal volume of saline solution. Throughout the investigative period, weekly recordings of fasting blood glucose and body mass were meticulously documented. Subsequent to 8 weeks of gavage administration, retinal functionality was evaluated through fluorescence fundus angiography (FFA), flash electroretinogram (FERG), and optical coherence tomography (OCT). After 48 h post-evaluation, the mice were euthanized for ensuing experimentation.

2.2 Culture of primary RGCs

Primary RGCs were isolated from the retina of C57BL/6 mice on the 5th day after birth. After being disinfected with 75% ethanol by volume fraction, the mice were euthanized by cervical spondylolysis. The eyeballs were separated using sterile micro toothless forceps, rinsed in sterile PBS to remove blood stains, and transferred to complete DMEM/F12. The retina was separated under an anatomical microscope and placed in a cell culture box for enzymatic hydrolysis for 20 min. Then discard the supernatant, rinse with complete DMEM/F12 3 times, add complete DMEM/F12, gently blow the retina about 50 times with a glass tube to prepare the cell suspension, count the cells with a blood cell counting plate, adjust the cell suspension density to 15×10^6 cell/mL with complete DMEM/F12, and inoculate it to 2 mL/well on a 6-well plate. Observe the cell concentration and adhesion of each well under an inverted electron microscope. Place at 37 ℃, with a volume fraction of 5% CO_2, and incubate for 24 h in a primary culture incubator. The cells were identified with poudomain transcription factor (Brn3a) (1:500, ab245230, Abcam, USA). Inorder to simulate DR, the cells were cultivated in medium equipped with 50 mmol/L high glucose for 48 h. In order to eliminate the influence of high glucose (HG) osmotic pressure on the experiment, we set up a Mannose group, and the concentration of Mannose was consistent with that of HG. At the same time, the different doses of Sal (5, 10 and 20 μmol/L), ferrostatin-1 (ferroptosis inhibitor) (Fer-1, 5 μmol/L) and HIF-1α inhibitor PX-478 (25 μmol/L) and the activator $CoCl_2$ (50 μmol/L) were added for 48 h. Sal, Fer-1, PX-478, and $CoCl_2$ were all dissolved in dimethyl sulfoxide to an appropriate concentration.

2.3 Retinal structure and function detection

2.3.1 FFA

Subsequent to routine anesthesia (3 mL/kg 1% pentobarbital sodium and 20 μL 10% xylazine hydrochloride injection and induction of mydriasis using compound tropicamide, mice were administered an intraperitoneal injection of 1.7 mL/kg 2% fluorescein sodium. This procedure facilitated the scrutiny of any fundus lesions and potential fluorescein leakage within the mice.

2.3.2 FERG

The Visual Electrophysiology Instrument (OPTO-ERG, Optoprobe Science Ltd., UK) was employed in accordance with the operating system's guidelines. The amplitudes of b-waves and oscillatory potentials (Ops) were systematically recorded for subsequent statistical analysis.

2.3.3 OCT

The retinal structure got investigated using the Ultramicro Ophthalmol Imaging System (ISOCT, Optoprobe Science Ltd., UK),

adjusting the light source to concentrate on the retina. Following the culmination of the experiment, the eyes were flushed with saline and safeguarded against infection with levofloxacin eye drops. The retinal thickness got analyzed utilizing OCT Image Analysis software (Version 2.0).

2.3.4 Hematoxylin and eosin (HE) staining

HE staining got conducted in conformity with the manufacturer's protocols (Solarbio, Beijing, China). Photographic evidence got obtained using an inverted fluorescence microscope (Olympus, Japan), at 300 μm from the optic nerve. The relative retinal thickness (relative to control) got measured between retinal ganglion cell layer (GCL) to outer nuclear layer (ONL). Additionally, RGCs count in the GCL got quantified within each field of view.

2.4 Apoptosis detection

TUNEL staining got executed following the guidelines of the TUNEL apoptosis assay kit (Roche, USA). Imagery got captured 300 μm from the optic nerve with an inverted fluorescence microscope (Olympus, Japan). The TUNEL staining-positive cells count in each field of view got subsequently counted. For flow cytometry, cultured RGCs cells were processed as per the manufacturer's protocols (Solarbio, Beijing, China), and then analyzed utilizing a flow cytometer (NOVOCYTE 2060, ACEA, USA).

2.5 Transmission electron microscopy (TEM) to observe the intrinsic structure of RGCs

Retinal specimens were procured from mice thoroughly anesthetized with 0.3% pentobarbital sodium (0.2 mL/10 g). The eyes were excised and the retinas isolated under a stereomicroscope (SZ51, Olympus, Japan), then preserved in 2.5% glutaraldehyde (G1102, Servicebio, Beijing, China) for 2 h at 4 ℃.

For cellular samples, RGCs got cultured in 6-well plates at 3×10^5 cells/well for a whole day, after that was an incubation with HG, Sal (10338-51-9, Dalian Meilun Biotech Co. Ltd., China), and Fer-1 (347174-05-4, Sigma, USA). Subsequently, the cells got fixed by 2.5% glutaraldehyde (P1126, Servicebio, Beijing, China) for 24 h, immersed in 1% osmium fixative at ambient temperature for 3 h post-PBS wash, and subjected to conventional dehydration, infiltration, and embedding. Ultimately, ultrathin sections with thickness ranged from 60 to 80 nm got sectioned, doubly stained by uranium-lead, post examined under a transmission electron microscope (Hitachi, HT7700) for image acquisition and analysis.

2.6 Immunohistochemical staining

Upon completion of the dewaxing and hydration process, paraffin sections got exposed to 0.01 mol/L sodium citrate buffer solution (pH 6.0) for high-pressure antigen retrieval. Subsequently, we incubated the sections with 3% H_2O_2 at ambient temperature for a period of 10 min, safeguarded from exposure to light, and then blocked for a 30-min duration utilizing 10% goat serum. Following this preparatory step, sections got subjected to overnight incubation at 4 ℃ with specific antibodies targeting glutathione peroxidase 4 (GPX4) (1:300, DF6701, Affinity) and solute carrier family 7, member 11 (SLC7A11) (1:500, ab307601, Abcam). After a rewarming period of 45 min, and subsequent washing with PBS, sections got treated with HRP-linked secondary antibodies (1:500, ab6721, Abcam) for 30 min. Chromogenic detection got facilitated using DAB, with nuclei counterstained by hematoxylin. The final preparations got methodically photographed and evaluated using an optical microscope.

2.7 Immunofluorescence

For the retina: subsequent to dewaxing and hydration, paraffin sections got exposed to 0.01 mol/L sodium citrate buffer solution (pH 6.0) for the purpose of high-pressure antigen retrieval. We subsequently permeabilized the sections by 0.3% Triton X-100 for a span of 15 min, then blocked them by 10% goat serum for 1 h at ambient temperature. Following these procedures, sections got incubated at 4 ℃ for a whole night with antibodies against HIF-1α (1:500, H1alpha67, Abcam) and Brn3a (1:500, ab245230, Abcam). Following a PBS wash, fluorescent secondary antibodies got utilized and incubated for 2 h at room temperature, shielded from light. Finally, sections got mounted, photographed, and scrutinized using fluorescence microscopy.

RGCs got subjected to the treatment process delineated earlier. The cells got permitted to adhere and subsequently fixed with 4% paraformaldehyde for a duration of 30 min at ambient temperature. Following this, the cells underwent incubation within 0.3% Triton X-100 for 15 min. After a blocking phase utilizing 10% goat serum at room temperature for 1 h, the cells got subjected to overnight incubation at 4 ℃ with specific antibodies against GPX4 (1:400, DF6701, Affinity), SLC7A11 (1:200, ab307601, Abcam), and HIF-1α (1:500, ab1, Abcam). Post PBS wash, the incubation process got carried out in the dark at room temperature for 2 h with fluorescent secondary antibodies. Following another PBS wash, the cells got sealed, captured photographically, and then examined under fluorescence microscopy.

2.8 Western blot analysis

Retinal or cellular specimens from the respective groups got harvested and subjected to lysis utilizing RIPA lysis solution, followed by the quantification of protein concentration *via* the BCA method. Thereafter, 10% SDS-PAGE gels got formulated, and 10 μL of protein got loaded into each well for the purpose of electrophoresis. Upon the completion of electrophoresis, proteins got conveyed to PVDF membranes, subsequently obstructed with 1% bovine serum albumin (BSA) for a 2-h period. Primary antibodies against GPX4 (1:1 000, DF6701, Affinity), SLC7A11 (1:2 000, ab307601, Abcam), HIF-1α (1:1 000, ab1, Abcam), and heme oxygenase-1 (HO-1) (1:5 000, ab189491, Abcam) got introduced, and the membranes underwent incubation at 4 ℃ for a whole night, with agitation. After a TBST wash, membranes got further incubated by horseradish peroxidase (HRP)-coupled secondary antibodies for 2 h. Subsequent treatment with ECL luminescent solution facilitated the visualization of protein bands. These bands got imaged, and their grayscale values analyzed utilizing ImageJ software, *β*-actin being employed as the loading control.

2.9 Cell counting kit-8 (CCK8) assay

RGCs cells were allocated to 96-well plates at 4×10^3 cells/well. Following attainment of the logarithmic growth phase, the medium

got removed, and cells were subjected to high glucose concentrations (25, 50, 100 mmol/L) for intervals of 24, 48, and 72 h. Sequentially, medium containing different Sal concentrations got introduced, with normal control receiving a same volume of standard medium. A total of 3 distinct wells got designated for each Sal treatment. Next, 10 μL of CCK8 solution was introduced into each well, and the plates were incubated at 37 ℃ for 1 h. The subsequent evaluation of cell viability got conducted employing CCK8 (CK04, Servicebio, Beijing, China).

2.10 Lactate dehydrogenase (LDH) release assay

Intracellular LDH concentrations got evaluated in conformity with the LDH cytotoxicity assay kit protocol (BC0685, Servicebio, Beijing, China).

2.11 Reactive oxygen species (ROS) level detection

Animal Samples: fresh retina by staining with dihydroethidium (DHE) staining solution (ID3560, Servicebio, Beijing, China) in frozen state 15 min, which got diluted at a 1:100 ratio. Cell samples: subsequently, the cells were incubated in a medium containing HDCF-DA (final concentration 10 μmol/L) for 30 min at 37 ℃, shielded from light. For ROS analysis, the green fluorescence was quantitatively assessed by measuring its intensity at 530 nm wavelength.

2.12 Lipid peroxidation and antioxidant capacity assays

Malondialdehyde (MDA), glutathione (GSH) levels, and superoxide dismutase (SOD) activity in both retinal tissue and cellular samples were assessed following the provided kit instructions from the manufacturer (Servicebio, Beijing, China).

2.13 Detection of mitochondrial membrane potential (MMP)

RGCs got allocated to 6-well plates at 3×10^5 cells/well and underwent incubation for a 24 h duration. Subsequently, cells got exposed to HG, Sal, and Fer-1. The assessment of MMP got carried out by calculating the MMP by comparing the levels of green fluorescence (JC-1 monomer) at 530 nm with those of red fluorescence (JC-1 polymer) at 590 nm.

2.14 Retinal and Fe^{2+} level detection in RGCs cells

In accordance with the iron assay kit protocol (ab83366, Abcam), the supernatant got meticulously removed, followed by the measurement of absorbance at 593 nm utilizing an enzyme marker (Multiskan GO, Thermo, USA). The data got then integrated into the iron assay kit Excel sheet to calculate the Fe^{2+} concentration. Following a 48 h infection with HAdV-7 at 10 mol/L, cells got treated with an HBSS solution containing 1 μmol/L of FerroOrange (MX4559-24UG, UK Bio, Shanghai, China). Fluorescence assessments were carried out utilizing a fluorescence microscope, and the intensity of fluorescence was quantified through the utilization of ImageJ software.

2.15 Predication of Sal action targets

Unrevealed downstream factors of Sal got initially retrieved from the GeneCards® (https://www.genecards.org/), utilizing a ranking mechanism based on scores (top 5 genes), and subsequently cross-referenced with the STITCH database (http://stitch.embl.de/). The intersection of these data was ascertained employing venny 2.1.0 software.

2.16 Sal and HIF-1α molecular docking experiments

The 3D structure of Sal, in SDF format, got retrieved from the PubChem database utilizing its respective CAS number. The protein structure of HIF-1α (PDB ID: 4H6J) was procured from the Protein Data Bank (PDB)database. The protein binding site was predicted utilizing POCASA 1.1, and docking was executed with AutoDock Vina1.1.2. The interaction pattern of the docking results were scrutinized employing PyMOL2.3.0.

2.17 Surface plasmon resonance (SPR) assay

To confirm the binding affinity of recombinant HIF-1α protein and Sal, SPR assay was performed with BIAcore T200 (Biacore, Cytiva), and the dissociation constant (K_D) value was calculated using BIAcore T200 analysis software.

2.18 Statistical analysis

Grayscale values of protein bands, the number of RGCs, the quantity of TUNEL staining positive cells, the percentage of immunohistochemical DAB color development area, and the intensity of immunofluorescence got analyzed utilizing ImageJ software. GraphPad Prism 8 got employed for the construction of statistical analysis graphs. The data got processed and articulated as mean ± SEM, employing SPSS 23.0 statistical software. Comparisons between multiple samples got executed utilizing one-way ANOVA, whereas comparisons between 2 distinct groups were undertaken using an independent samples *t*-test. A *P*-value below 0.05 was deemed to signify statistically significant differences.

3. Results

3.1 Effects of Sal on fasting blood glucose and body weight in db/db mice

Relative to *db*/*m* mice, *db*/*db* mice demonstrated markedly augmented blood glucose levels (Fig. 1A). Such an augmentation was, however, ameliorated by Sal, leading to a diminution in blood glucose levels in the mice (Fig. 1A). The weight of the mice in the *db*/*m* and *db*/*m* + Sal cohorts progressively increased, whereas that of the mice in the *db*/*db* and *db*/*db* + Sal groups displayed a declining trend subsequent to the 17 weeks threshold. This pattern implied that Sal did not induce a significant alteration in mouse body weight (Fig. 1B). These results substantiate that Sal is efficacious in moderating blood sugar levels in mice.

3.2 Sal improved visual function in db/db mice

To investigate the effect of Sal on visual function in mice, fundus photography and FFA examination got conducted. The findings revealed an absence of retinal vascular tortuosity or pronounced fluorescent regions in 20-week *db*/*db* mice, signifying minimal

neovascularization and vascular leakage in these subjects (Fig. 2A). FERG assays were implemented, wherein b-wave amplitudes and Ops serve as sensitive markers of early DR. Data indicated considerably attenuated b-wave amplitudes and Ops in *db/db* mice at the 20-week interval (Figs. 2B–D). These measures, however, got significantly augmented post Sal intervention (Figs. 2B–D), suggesting that Sal may efficaciously alleviate visual impairment in *db/db* mice.

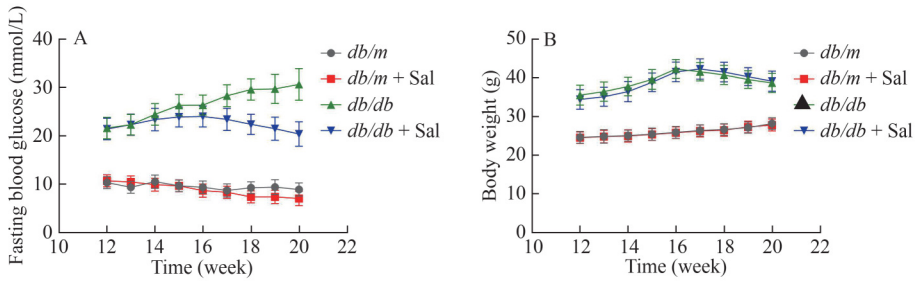

Fig. 1 Influence of Sal on fasting blood glucose and body weight in *db/db* mice (n = 12). (A) Fasting blood glucose. (B) Body weight.

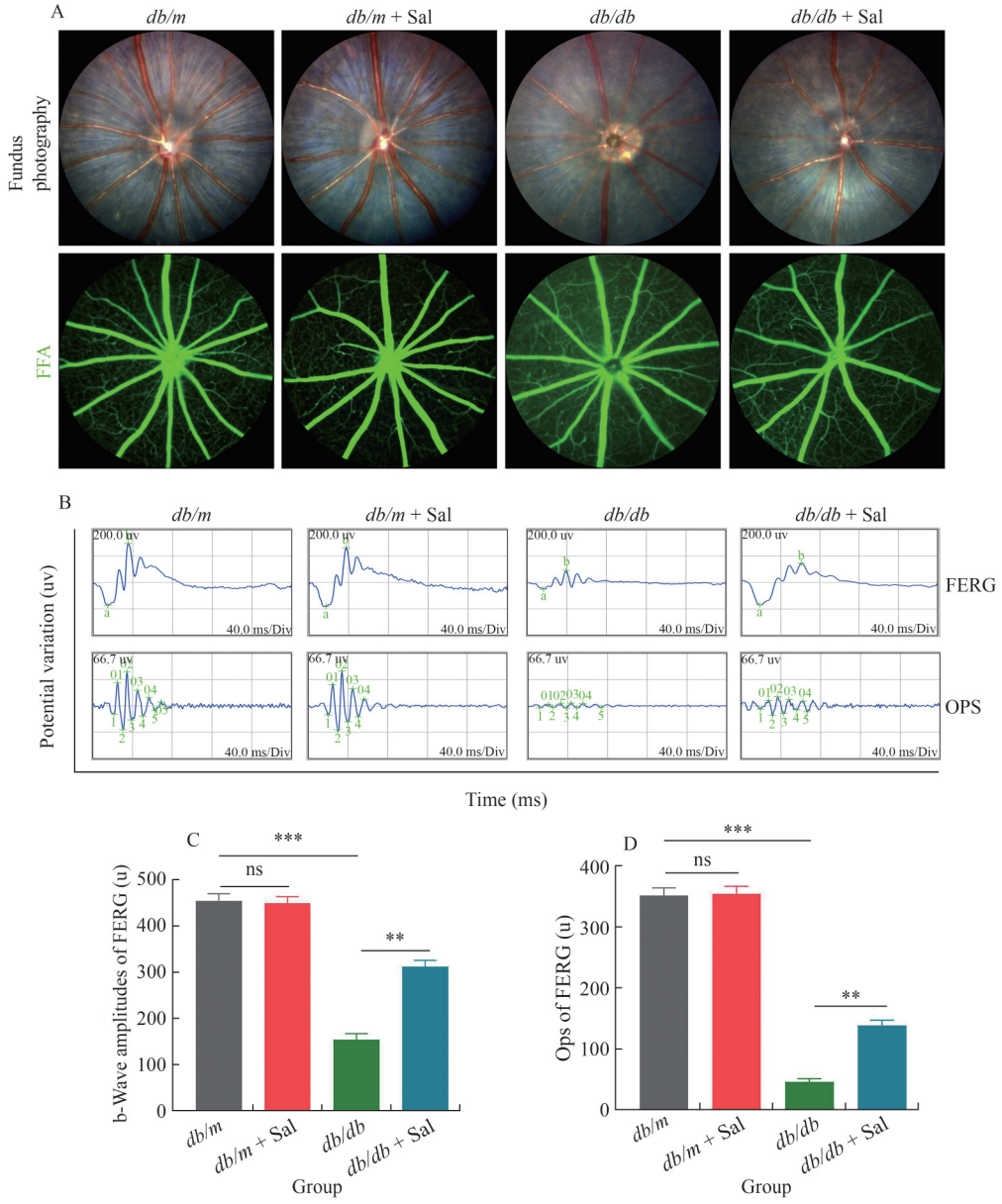

Fig. 2 Sal augments visual function in *db/db* mice (n = 5, ≥ 3 individual experiments). (A) Fundus photography and FFA of mice. (B) FERG. (C) b-Wave amplitudes of FERG. (D) Ops of FERG. ns (not significant) when $P > 0.05$, $^{**}P < 0.01$, and $^{***}P < 0.001$.

3.3 Sal improved retinal neuropathy in db/db mice

To verify the effect of Sal on retinal neuropathy. Analysis from OCT, HE staining, and TUNEL staining exhibited that *db/db* mice harbored distorted retinal architecture, significantly contracted retinal thickness and RGCs number, along with conspicuous apoptosis of RGCs (Fig. 3). These outcomes implied that microangiopathy got absent at the 20-week mark in *db/db* mice, though neurological detriment had already manifested. Conversely, retinal thickness and RGCs number markedly elevated following Sal treatment, and RGCs apoptosis got notably restrained (Fig. 3). Such findings propose that Sal could effectively attenuate retinal neuropathy in *db/db* mice.

3.4 Sal reduced the level of oxidative stress and lipid peroxidation in the retina of db/db mice

In light of Sal's pronounced anti-oxidative stress properties, an investigation got embarked upon to elucidate the potential of Sal in modulating retinal oxidative stress and lipid peroxidation levels in *db/db* mice. Through the utilization of DHE staining and MDA kits, both retinal ROS levels and MDA content got ascertained. The data revealed a significant elevation in retinal ROS levels and MDA content in *db/db* mice, a phenomenon strikingly mitigated following Sal administration (Figs. 4A–C). Subsequent analyses of GSH, a fundamental antioxidant within animal cells, and SOD, an indispensable antioxidant enzyme in organisms, disclosed a considerable decline in retinal GSH and SOD activities in *db/db* mice, which got nevertheless restored by Sal intervention (Figs. 4D and E). The collective evidence thereby posits that Sal is capable of suppressing both ROS and MDA levels while augmenting GSH and SOD levels, thereby exhibiting an inhibitory effect on oxidative stress and lipid peroxidation-induced damage within the *db/db* mice retinas.

3.5 Sal reduced RGCs ferroptosis in db/db mice

Ferroptosis, an iron-dependent cellular demise recently identified, poses an enigmatic role in DR, with morphological mitochondrial transformations being its most indicative feature. TEM evaluations

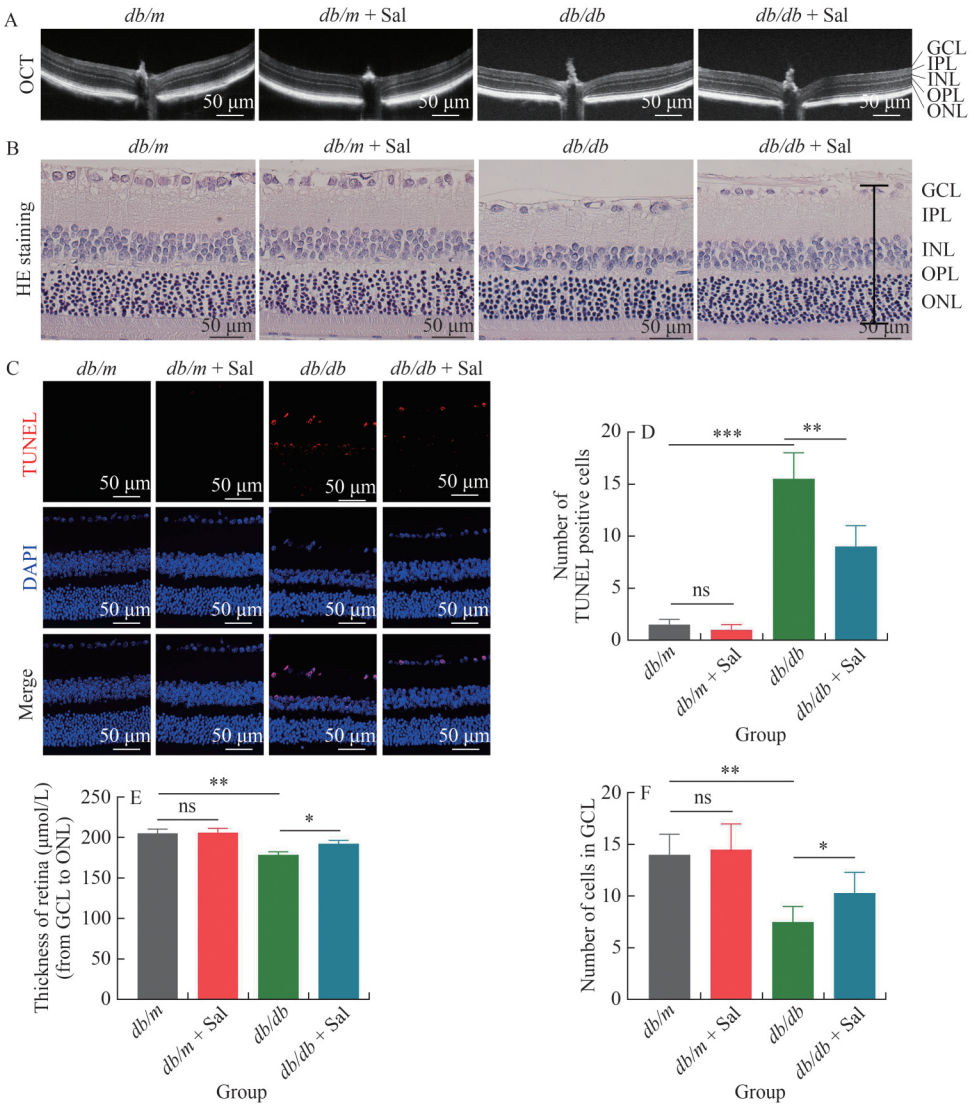

Fig. 3 Sal mitigates retinal neuropathy in *db/db* mice ($n = 5, \geq 3$ individual experiments). (A) OCT. (B) HE staining. (C) TUNEL staining. (D) Enumeration of TUNEL staining positive cells. (E) Retinal thickness (from GCL to ONL). (F) RGCs count. Scale bar = 50 μm. ns (not significant) when $P > 0.05$, $^{*}P < 0.05$, $^{**}P < 0.01$, and $^{***}P < 0.001$.

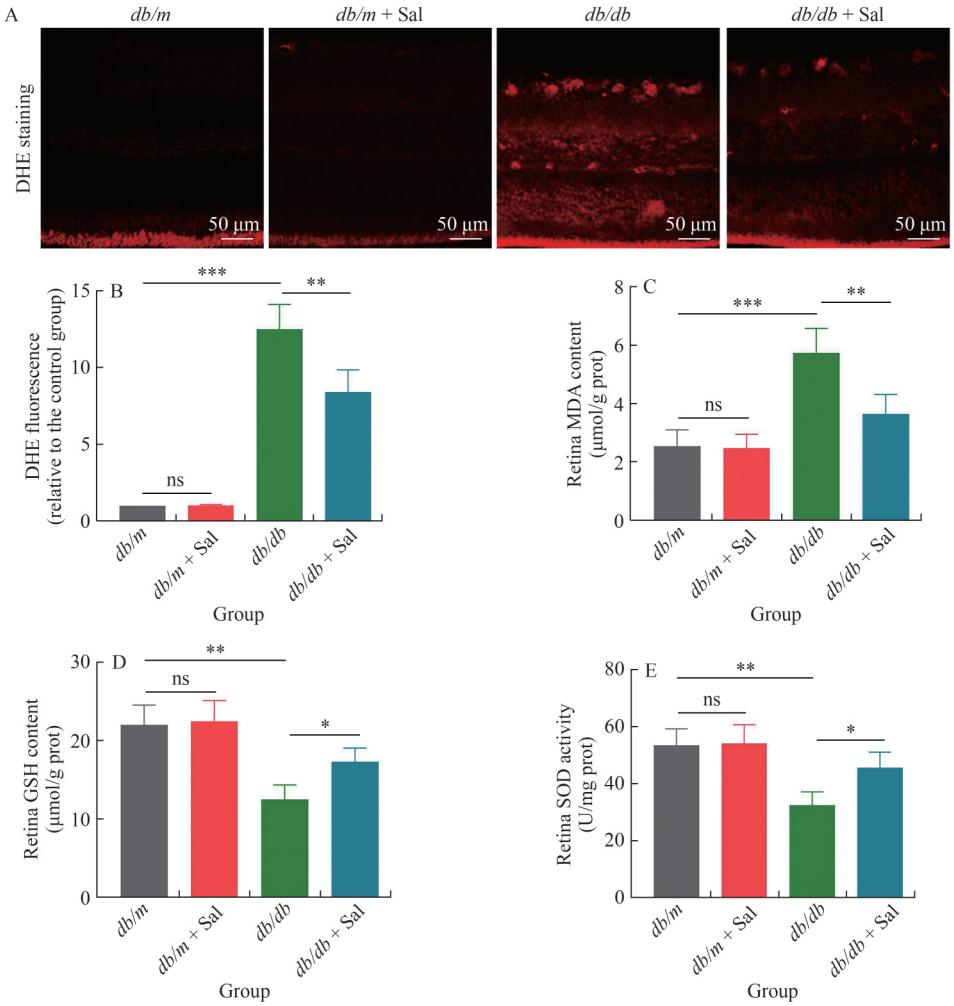

Fig. 4 Sal mitigates oxidative stress and lipid peroxidation in the retinas of *db/db* mice ($n = 5, \geq 3$ individual experiments). (A) DHE staining. (B) DHE fluorescence assessment. (C) Retinal MDA quantification. (D) Retinal GSH concentration. (E) Retinal SOD enzymatic activity. Scale bar = 50 μm. ns (not significant) when $P > 0.05$, $^{*}P < 0.05$, $^{**}P < 0.01$, and $^{***}P < 0.001$.

unearthed constricted RGCs mitochondria within *db/db* mice, typified by a densified membrane and diminished cristae (Fig. 5A). However, a juxtaposition with Sal-treated RGCs mitochondria revealed a relatively normal appearance and more defined cristae (Fig. 5A). Since Fe^{2+} is instrumental in precipitating ferroptosis, retinal Fe^{2+} concentrations got assessed, revealing a discernible increment within *db/db* mice, which got notably counteracted by Sal (Fig. 5F). Moreover, examinations got conducted on the GPX4 enzyme, a unique intracellular GSH peroxidase utilized for liposome peroxide reduction, it's noteworthy that the downregulation of SLC7A11, a crucial amino acid transport protein and an essential regulator of ferroptosis, can indirectly hinder GPX4 activity. This obstruction occurs through interference with the cysteine metabolic pathway, resulting in reduced intracellular cystine levels and subsequent depletion of GSH synthesis. These alterations culminate in the accumulation of lipid peroxides and the initiation of cell ferroptosis. Western blot and immunohistochemical assays denoted that GPX4 and SLC7A11 expressions got conspicuously suppressed within the retinas of *db/db* mice, yet upregulated post-Sal treatment (Figs. 5B–E). These collective findings assert that ferroptosis constitutes a salient pathological pathway for RGCs damage in *db/db* mice, and Sal exerts a tangible inhibitory effect on RGCs ferroptosis within these mice.

3.6 Sal reduced HG-induced damage in RGCs

To elucidate the impact of HG on cellular viability and LDH secretion in RGCs, initial treatment with HG got executed, followed by an analytical application of CCK-8 and LDH assays. The findings illustrated a dose-dependent decrement in RGCs cell viability (25, 50, 100 mmol/L) and a corresponding enhancement in LDH release at intervals of 24, 48, and 72 h (Figs. 6A and B). Based upon these primary observations, a HG concentration of 50 mmol/L and an exposure duration of 48 h got selected for subsequent experimentation. These data provide evidence that HG is capable of attenuating cell viability while concurrently escalating LDH release. Meanwhile, in order to eliminate the influence of HG osmotic pressure on the experiment, we set up a Mannose group, and the concentration of Mannose was consistent with that of HG. In evaluating Sal's potential to shield against injuries induced by HG in RGCs, and in ascertaining the correlation between Sal concentration and cellular viability and LDH concentration, RGCs got pretreated by graded concentrations of Sal for 4 h preceding HG administration, followed by execution of CCK-8 and LDH assays. The ensuing results depicted an augmented cell viability in correspondence with an increased Sal concentration, and a dose-dependent (5, 10, 20 μmol/L) suppression

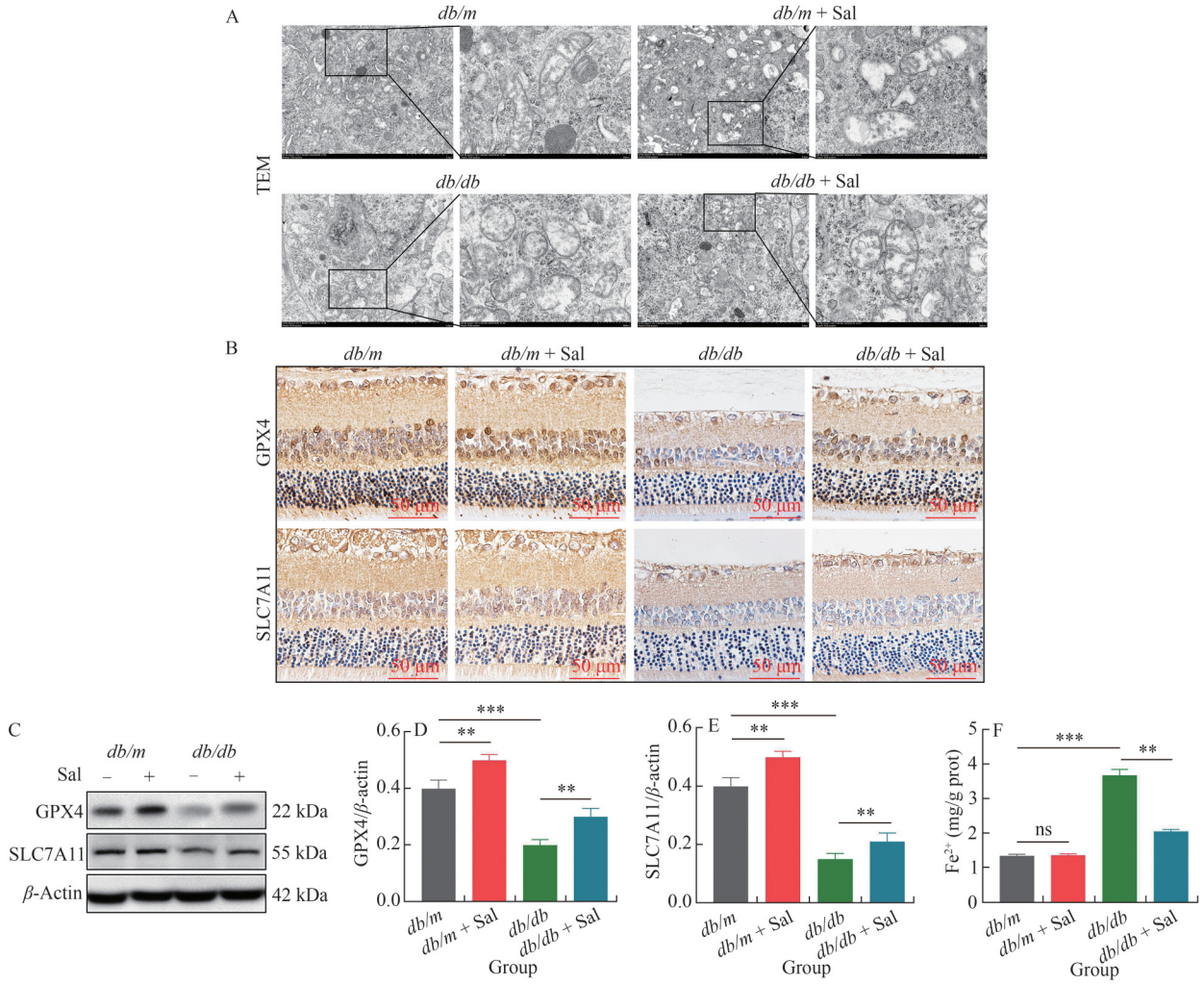

Fig. 5 Sal diminishes *db/db* mice RGCs ferroptosis ($n = 5, \geq 3$ individual experiments). (A) Ultrastructural alterations in RGCs visualized by TEM. (B) Immunohistochemical detection of GPX4 and SLC7A11. (C) GPX4 and SLC7A11 expression by Western blotting. (D) Relative expression of GPX4. (E) Relative expression of SLC7A11. (F) Fe^{2+} quantification. Scale bar = 50 μm. ns (not significant) when $P > 0.05$, $^{**}P < 0.01$, and $^{***}P < 0.001$.

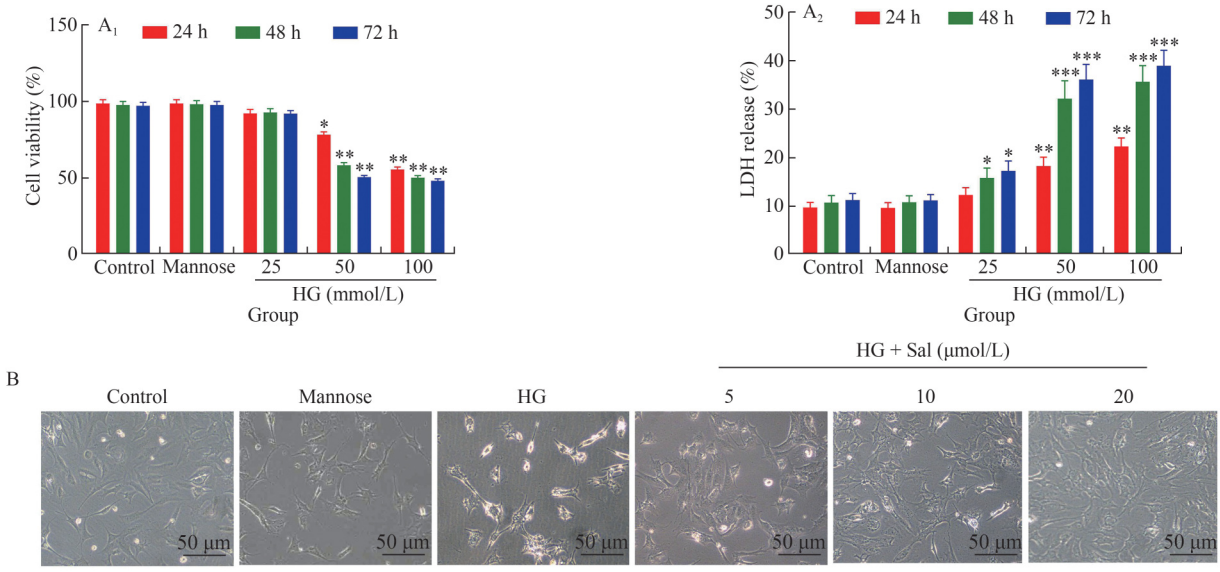

Fig. 6 Sal mitigates HG-induced damages in RGCs ($n = 3, \geq 3$ individual experiments). (A) Influence of HG on cell viability and LDH discharge within RGCs. (B) Impact of Sal on RGCs cellular status. (C) Flow cytometry quantification of RGCs apoptosis. (D) Influence of Sal on RGCs viability. (E) Impact of Sal on LDH release in RGCs. (F) RGCs apoptotic rate assessment. Concentration of Mannose: 50 mmol/L; concentration of HG: 50 mmol/L. Scale bar = 50 μm. ns (not significant) when $P > 0.05$, $^{*}P < 0.05$, $^{**}P < 0.01$, and $^{***}P < 0.001$.

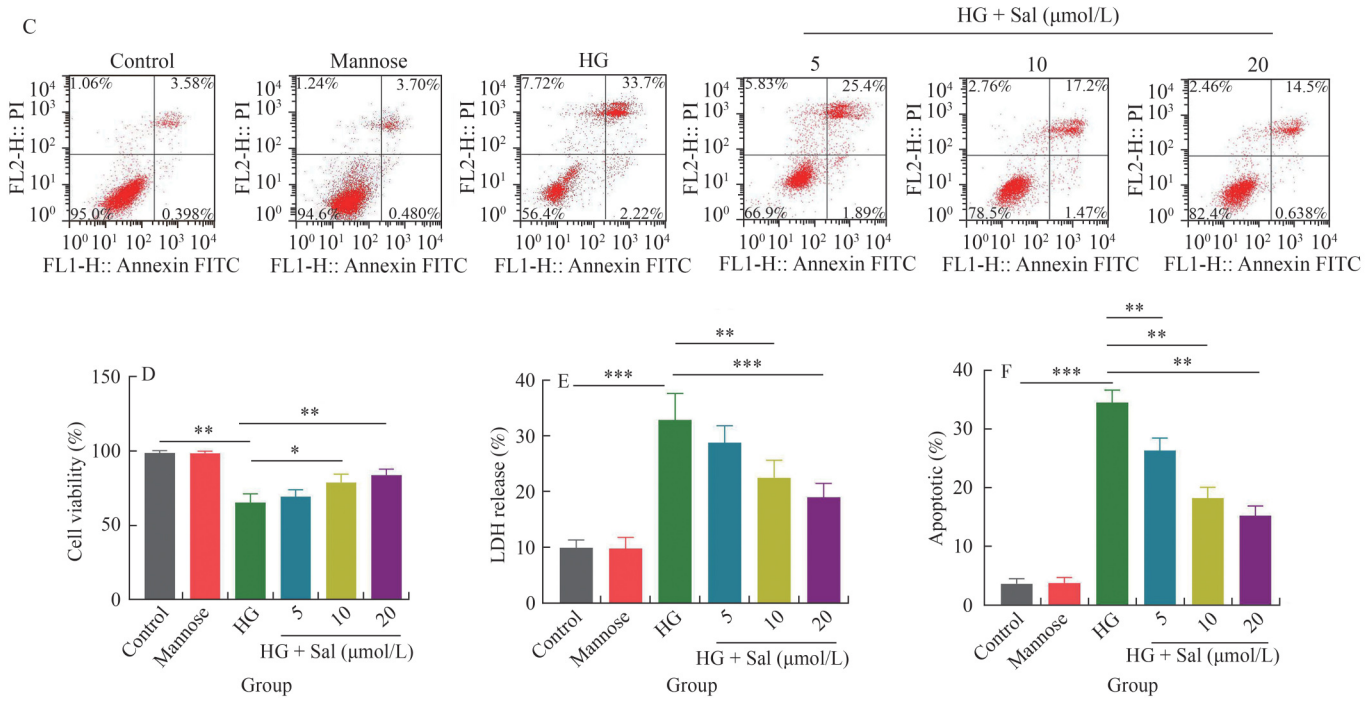

Fig. 6 (*Continued*)

of LDH release by Sal (Figs. 6E and F). Utilizing flow cytometry to assess Sal's suppressive action on HG-induced RGCs mortality, it got ascertained that Sal inhibited apoptosis in a dose-dependent fashion (Figs. 6D and G). These insights collectively suggest that Sal has the ability to bolster cell viability, diminish LDH release, and inhibit apoptosis. Based upon these primary observations, a Sal concentration of 20 μmol/L got selected for subsequent experimentation.

3.7 Sal reduced HG-induced oxidative stress and lipid peroxidation levels in RGCs

DCFH-DA probe coupled with flow cytometry got employed to quantify intracellular ROS concentrations, which got found to be significantly intensified subsequent to HG stimulation in RGCs cells but conspicuously attenuated following treatment with Sal and Fer-1 (Figs. 7A–D). An in-depth investigation into the antioxidant capacity and lipid peroxidation levels within RGCs cells revealed that HG led to a marked reduction in GSH and SOD activities and a substantial increase in MDA levels (Figs. 7E–G). In contrast, Sal and Fer-1 effectively revived GSH and SOD activities and appreciably reduced MDA concentrations (Figs. 7E–G). Therefore, these observations indicate that Sal possesses the capacity to decrease both ROS and MDA levels, and to enhance GSH and SOD levels, thereby manifesting significant inhibitory actions on oxidative stress created by HG and lipid peroxidation damage within RGCs.

3.8 Sal reduced HG-induced mitochondrial damage and RGCs ferroptosis

Mitochondrial functionality is commonly assessed through the evaluation of MMP, a measurement facilitated by JC-1 staining. The MMP level, ideally corresponding to the red/green fluorescence ratio, got observably diminished in RGCs cells following HG induction. This trend got significantly reversed upon administration of Sal and Fer-1 treatment (Figs. 8A and B). An orange iron probe, engineered to interact exclusively with Fe^{2+} within living cells, got employed to monitor Fe^{2+} accumulation. Fe^{2+} levels got found to be substantially elevated in RGCs cells subsequent to HG induction, but got

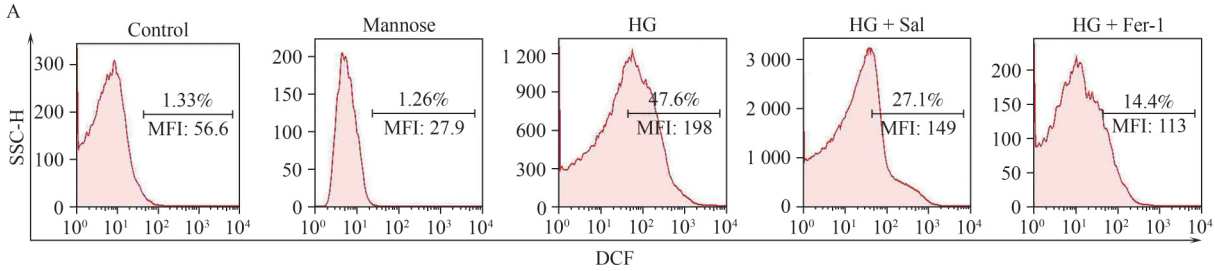

Fig. 7 Sal abates oxidative stress created by HG and lipid peroxidation levels within RGCs ($n = 3$, ≥ 3 individual experiments). (A) Flow cytometry quantification of RGCs ROS concentrations. (B) ROS count frequency. (C) DCFH-DA evaluation of RGCs ROS concentrations. (D) DCFH-DA fluorescence quantification. (E) MDA quantities in RGCs. (F) GSH quantities in RGCs. (G) SOD quantities in RGCs. Concentration of Mannose: 50 mmol/L; concentration of HG: 50 mmol/L. Concentration of Sal: 20 μmol/L; concentration of Fer-1: 5 μmol/L. Scale bar = 50 μm. ns (not significant) when $P > 0.05$, $^{**}P < 0.01$, and $^{***}P < 0.001$.

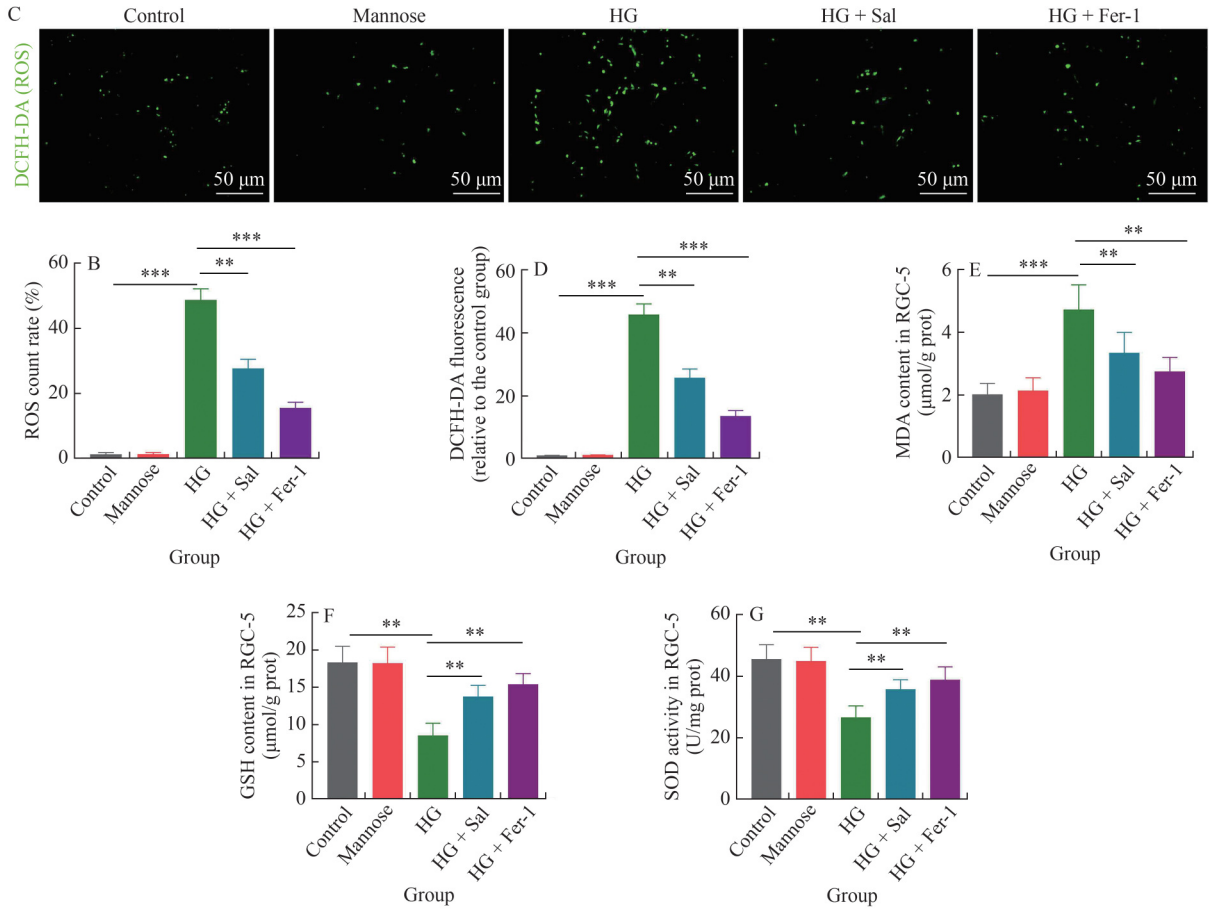

Fig. 7 (*Continued*)

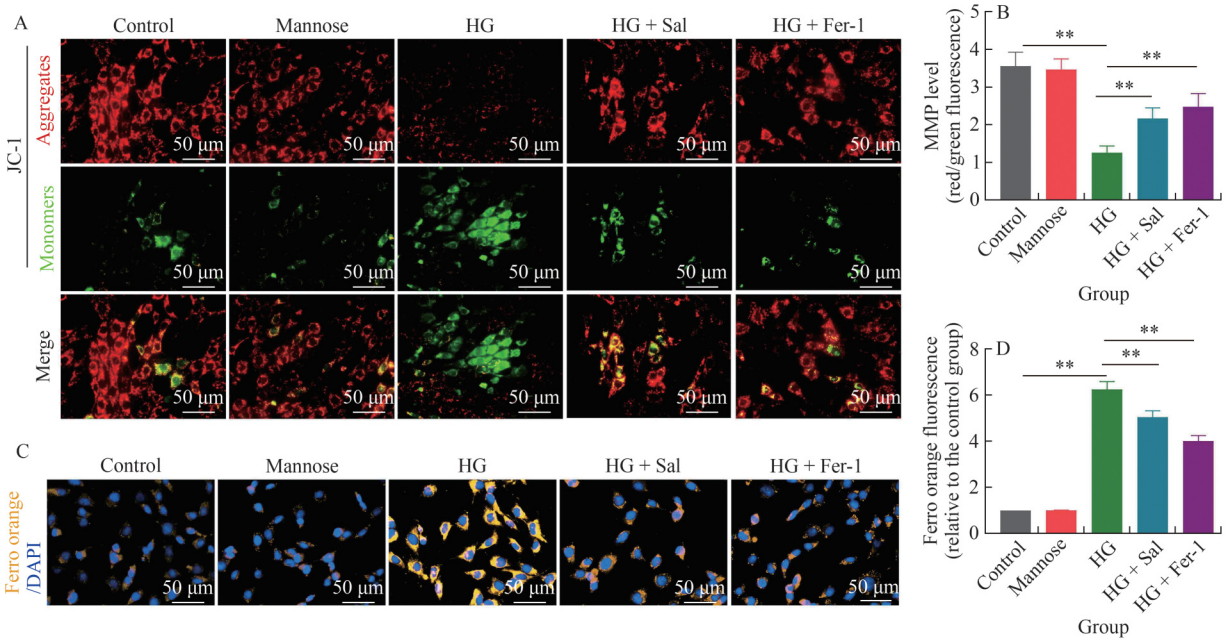

Fig. 8 Sal attenuates HG-induced mitochondrial damage and ferroptosis in RGCs ($n = 3$, ≥ 3 individual experiments). (A) JC-1 staining for MMP levels. (B) Quantitative analysis of MMP levels. (C) Ferro Orange. (D) Ferro Orange fluorescence analysis. (E) TEM examination of mitochondrial alterations in RGCs. (F) Detection of GPX4 and SLC7A11 expressions *via* Western blot. (G) Relative expression quantification of GPX4. (H) Relative expression quantification of SLC7A11. Concentration of Mannose: 50 mmol/L; concentration of HG: 50 mmol/L. Concentration of Sal: 20 μmol/L; concentration of Fer-1: 5 μmol/L. Scale bar = 50 μm. ns (not significant) when $P > 0.05$, $^{**}P < 0.01$, and $^{***}P < 0.001$.

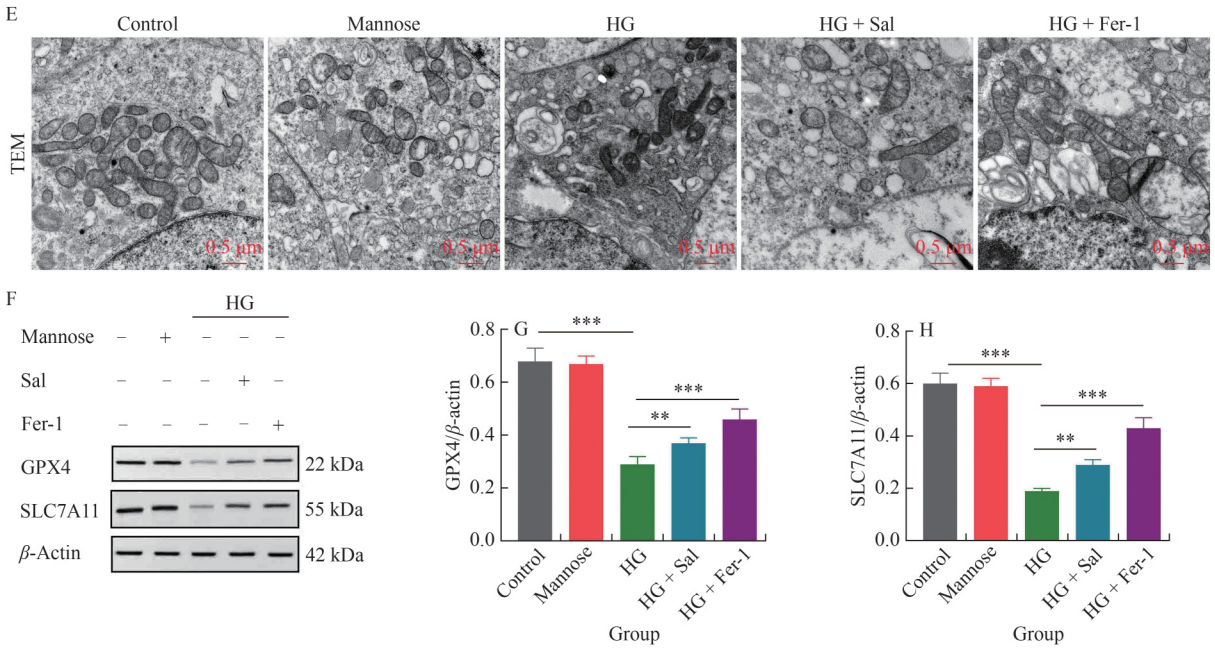

Fig. 8 (*Continued*)

noticeably reduced following Sal and Fer-1 treatment (Figs. 8C and D). Data gleaned from TEM illustrated that RGCs cells' mitochondria underwent contraction, an increase in membrane density, and a reduction in cristae subsequent to HG induction (Fig. 8E). Conversely, RGCs mitochondria treated with Sal and Fer-1 displayed near-normal morphology, clearly defined cristae (Fig. 8E). Western blot analysis underscored that the expressions of GPX4 and SLC7A11 got significantly downregulated in RGCs cells following HG induction (Figs. 8F–H), yet upregulated in response to Sal and Fer-1 treatment (Figs. 8F–H). These findings collectively suggest that Sal functions as a mitigative agent against HG-induced mitochondrial damage and ferroptosis in RGCs cells.

3.9 HIF-1α may serve as one of the pathways through which Sal contributes to its beneficial effects

The investigation into the underlying mechanisms by which Sal confers its beneficial effects entailed comprehensive bioinformatics analysis and molecular docking experiments for the prediction of Sal's targets. The outcomes thus acquired implicated HIF-1α as an integral target responsible for Sal's advantageous influences (Figs. 9A–C). Molecular docking is a theoretical simulation method for studying the interactions between molecules, such as drugs and receptors, and predicting their binding modes and affinities. Subsequent molecular docking studies ascertained that the binding energy of Sal with HIF-1α got −5.6 kcal/mol, an indication of efficacious binding. The interplay between Sal and HIF1α is predominantly mediated through the establishment of hydrogen bonds and hydrophobic interactions (Fig. 9D). Experimentally, SPR assays were carried out to verify the direct binding efficiency of Sal to HIF-1α. The mean K_D values of 8.451×10^{-5} for Sal-HIF-1α, indicated strong binding affinities (Fig. 9E).

To further delineate the spatial localization of HIF-1α within the mouse retina and elucidate Sal's modulatory influence upon it, immunofluorescence double-labeling got deployed to mark HIF-1α and RGCs. This procedure unmasked a pronounced co-localization of HIF-1α with RGCs, and the expression of HIF-1α got significantly escalated in the retina of *db/db* mice, whereas it got distinctly attenuated following Sal treatment (Fig. 9F). In HG-treated RGCs, the application of immunofluorescence to tag HIF-1α revealed that HIF-1α expression got noticeably increased, and entering the nucleus

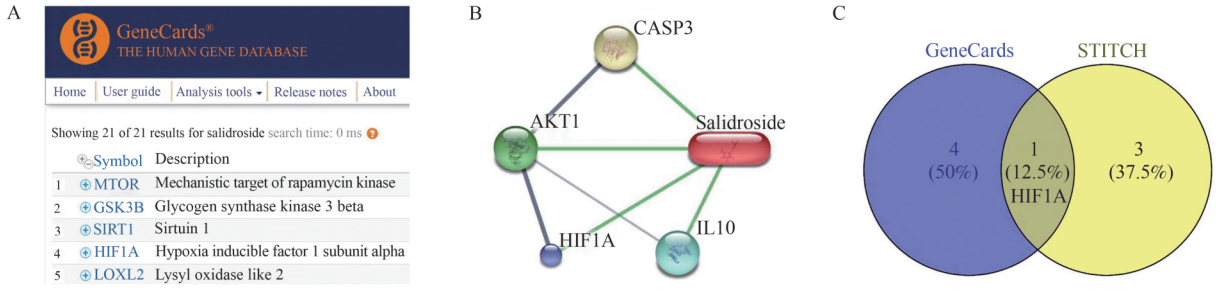

Fig. 9 HIF-1α as a potential mechanism underpinning Sal's beneficial effects ($n = 3, \geq 3$ individual experiments). (A) GeneCards database screening for Sal action targets. (B) STITCH database for Sal target prediction. (C) Venn analysis. (D) Molecular docking of Sal with HIF-1α. (E) SPR assay of the interaction between Sal and HIF-1α protein. (F) Immunofluorescence double-labeling of retinal HIF-1α and Brn3a. (G) Immunofluorescence of RGCs HIF-1α. (H) Western blot quantification of HIF-1α expressions. (I) Relative quantification of Cyto-HIF-1α. (J) Relative quantification of Nuc-HIF-1α. Scale bar = 50 μm. $^{**}P < 0.01$, and $^{***}P < 0.001$.

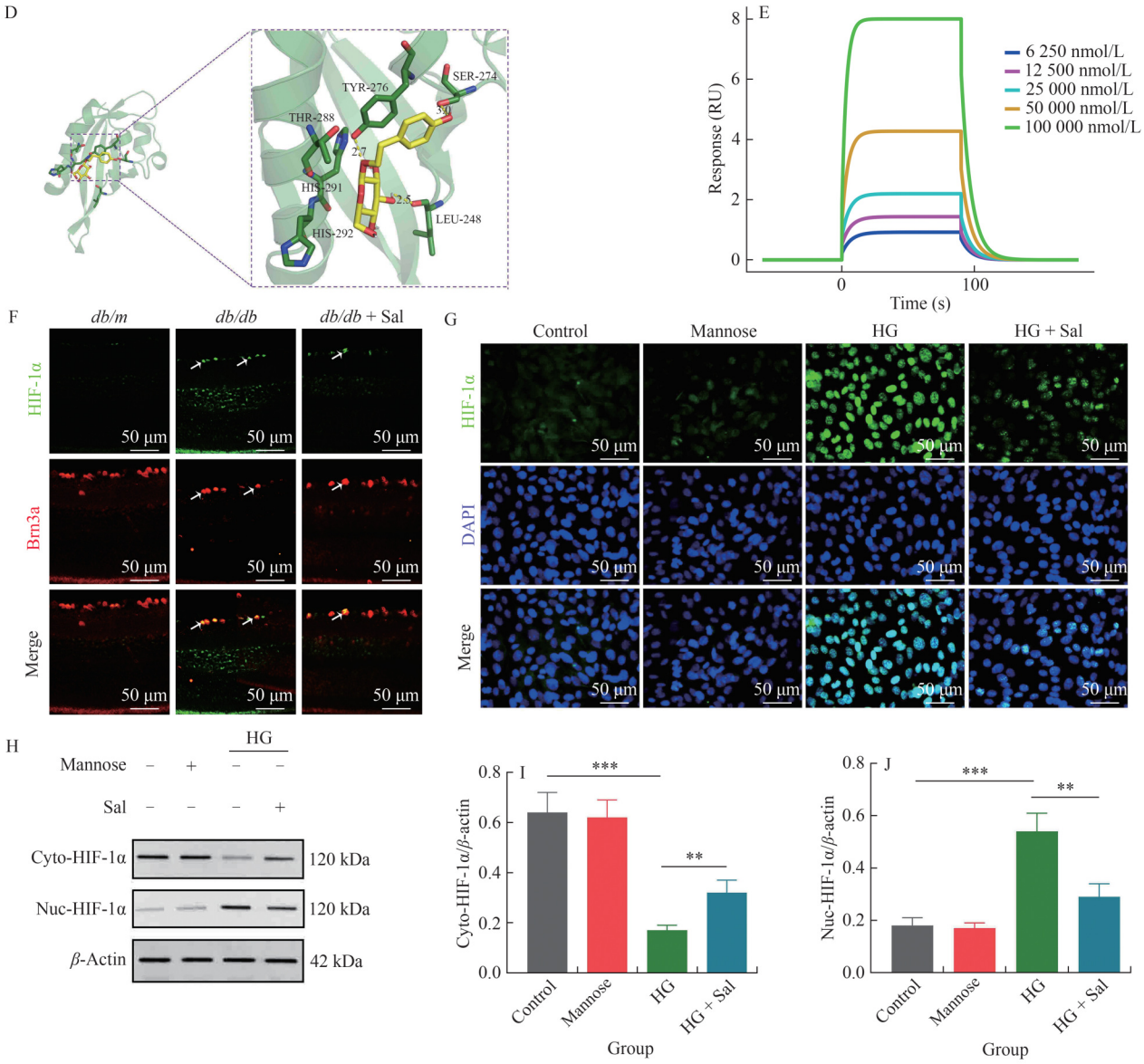

Fig. 9 (*Continued*)

increases. Conversely, Sal treatment markedly mitigated HIF-1α expression and reduce the expression of HIF-1α entering the nucleus (Fig. 9G). Considering that HIF-1α acts as a transcription factor by translocating to the nucleus, we further isolated the cytoplasmic and nuclear proteins of RGC and found that HIF-1α expression in the nucleus increased while HIF-1α expression in the cytoplasm decreased under HG state, Sal can inhibit the above changes (Figs. 9H–J). These observations intimate a close relationship between HIF-1α and RGCs ferroptosis, suggesting that HIF-1α may be one of the mechanisms by which Sal elicits its beneficial effects.

3.10 Sal inhibited HG-induced ferroptosis in RGCs via the HIF-1α/HO-1 pathway

In vivo analyses affirm that HIF-1α seemingly assumes a modulatory function in STZ-evoked retinal impairment. To evaluate whether the HIF-1α/HO-1 pathway functions as a probable conduit for Sal's advantageous effects, *in vitro* assessments got executed utilizing RGCs cells. These cells underwent preliminary treatment with the HIF-1α inhibitor PX-478 and the activator $CoCl_2$ for 4 h, followed by HG or Sal administration. JC-1 staining and TEM results show that Sal and PX-478 markedly increased the MMP level and improved the morphology of mitochondria (Figs. 10A–C). In addition, uncovering that Sal and PX-478 significantly reduced the expression of HIF-1α in the nucleus. HO-1 is a key molecule downstream of the HIF-1α signaling pathway, primarily responsible for breaking down heme to produce carbon monoxide, biliverdin, and free Fe^{2+}. When intracellular free Fe^{2+} overload occurs, it can trigger the Fenton reaction and ultimately induce ferroptosis. Therefore, we further tested the expressions of HO-1 and ferroptosis related proteins GPX4 and SCL7A11, and found that Sal and PX-478 can be downregulated HO-1 expression, markedly facilitated the expressions of GPX4 and SCL7A11 (Figs. 10D–I). Contrastingly, $CoCl_2$ abrogated Sal's anti-ferroptosis efficacy (Fig. 10).

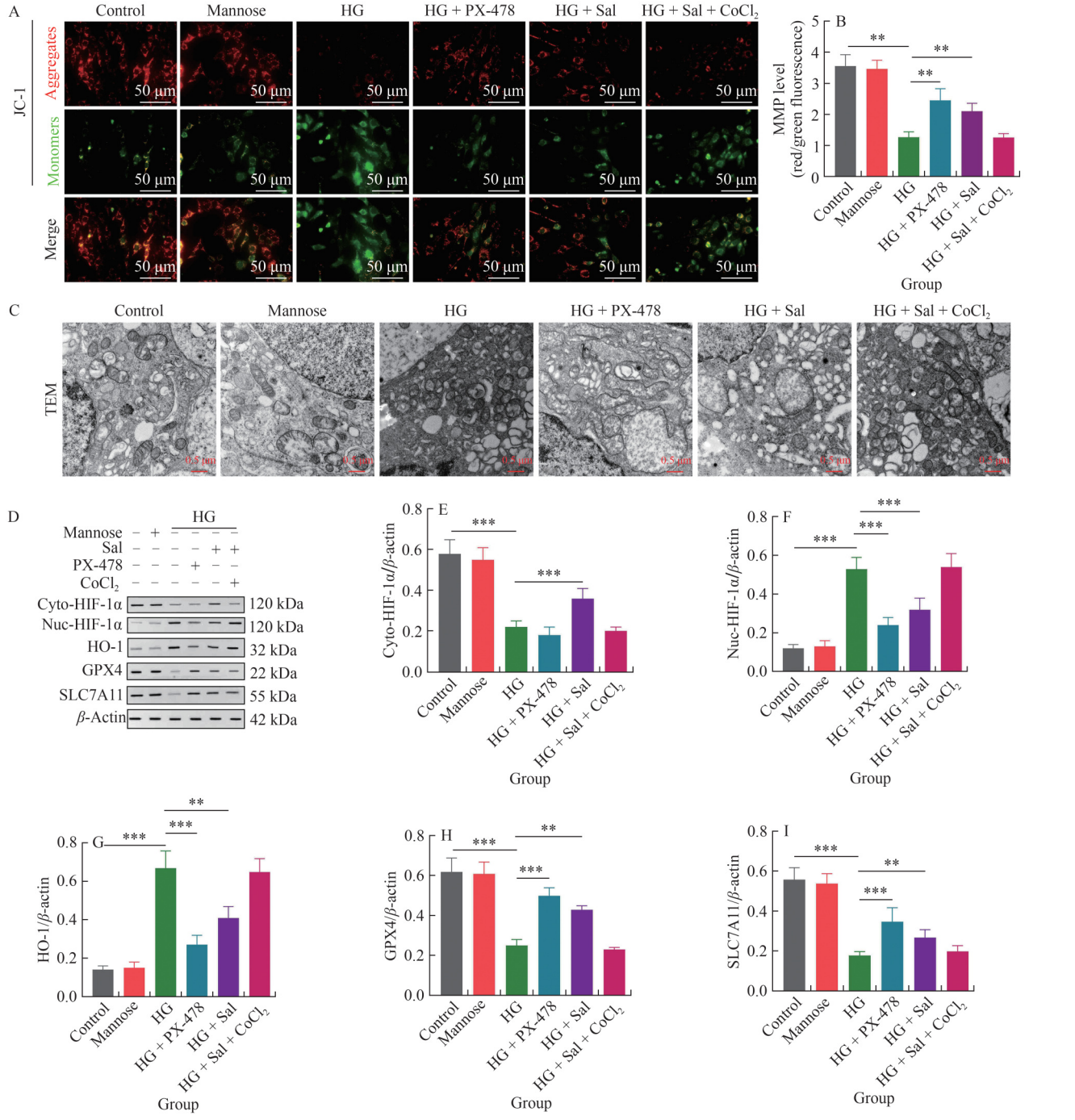

Fig. 10 Inhibition of HG-Induced ferroptosis in RGCs through the HIF-1α/HO-1 pathway by Sal ($n = 3, \geq 3$ individual experiments). (A) JC-1 staining for MMP levels. (B) Quantitative analysis of MMP levels. (C) TEM examination of mitochondrial alterations in RGCs. (D) Western blot quantification of HIF-1α, HO-1, GPX4, and SLC7A11 expressions. (E) Relative quantification of Cyto-HIF-1α. (F) Relative quantification of Nuc-HIF-1α. (G) Relative quantification of HO-1. (H) Relative quantification of GPX4. (I) Relative quantification of SLC7A11.

4. Discussion

The present investigation underscores that Sal confers neuroprotection against retinal trauma and HG-induced RGCs cellular injury in *db/db* mice. To explore further the modus operandi of Sal's prevention of RGCs ferroptosis, bioinformatics methodologies coupled with molecular docking experiments identified HIF-1α as a conceivable target for Sal's action. Subsequent *in vitro* findings posited that an HIF-1α inhibitor could obstruct HG-elicited RGCs ferroptosis, whereas the HIF-1α activator $CoCl_2$ could nullify Sal's protective impact. These insights propose that Sal mitigates retinal distress or HG-induced RGCs cellular damage in *db/db* mice, at least in part by constraining HIF-1α-mediated RGCs ferroptosis.

Through exhaustive examinations of DR, DR is now perceived to transcend mere microangiopathy, embodying a more intricate diabetic complication. Diabetic retinal neurodegeneration is acknowledged as a fundamental process in DR's early phases[17-18]. The current study revealed that *db/db* mice manifest structural irregularities in the retina

at 20 weeks, concomitant with notable decrement in retinal thickness, RGCs quantity, and appreciable RGCs apoptosis. The b-wave magnitudes and Ops in FERG also declined significantly. Conversely, fundus imaging and FFA findings did not manifest considerable neovascularization and vascular seepage, signifying that microangiopathy got absent at 20 weeks in *db/db* mice, while neurologic damage got already apparent. Consequently, the implementation of prompt prevention and treatment for neuropathic lesions emergent early in DR is vital. Recent innovations elucidate that the obstruction of IL-17RA averts RGCs apoptosis, hence impeding DR's advancement[19]. Viral overexpression of *D*-amino acid oxidase (DAAO) is potent in averting RGCs loss and blood-retinal barrier rupture in diabetic rats[20]. Moreover, intravitreal adenoviral conveyance of extraneous BDNF can revive RGCs death in the STZ rat paradigm[21]. MHY1485 has been shown to guard against RGCs loss in diabetes through autophagy blockade[22]. These collective findings endorse the notion that satisfactory measures have been taken to prevent and treat early neuropathy in DR.

A burgeoning compendium of empirical data elucidates that Sal manifests an array of multifaceted pharmacological properties. These encompass the attenuation of oxidative stress and inflammatory cascades, anti-ferroptosis activity, neuroprotection, and hypoglycemic and hypolipidemic functionalities. Sal exerts salient modulatory effects on a wide spectrum of pathologies, with a particular emphasis on diabetes and its ancillary complications[11,23]. Investigations have delineated that Sal ameliorates endothelial inflammation and oxidative stress in human umbilical vein endothelial cells (HUVECs), brought forth by advanced glycosylation end products (AGEs), through the intricate orchestration of the AMPK/NF-κB/NLRP3 signaling pathway[24]. The pivotal role of Sal in fostering angiogenesis and recuperation of blood perfusion in diabetic hindlimb ischemic mice, achieved by the inhibition of GPX4-mediated ferroptosis, has been validated[25]. Prior contributions from this research consortium have demonstrated that Sal mitigated cognitive dysfunction in diabetic rodents *via* the B3galt2/F3 signaling pathway[26], concurrently inhibiting the Act17-TRAF1-p6 MAPK pathway, hence opposing IL-17A-mediated ferroptosis in alveolar epithelial cells[27]. These aforementioned analyses furnish substantial theoretical substantiation for the present inquiry.

Within the purview of DR, the aberrant incitation of programmed cellular death conduits is discernible. Ferroptosis, a mode of cell death recently characterized, is defined by iron-catalyzed lipid peroxidation[28-29]. This distinct cellular demise cascade, disparate from apoptosis, autophagy, and other cellular death mechanisms, has been associated with an array of ocular maladies. The alleviation of RGCs ferroptosis curtailed retinal neuroinflammation in a murine model of retinal ischemia-reperfusion injury[30]. The anomalous agglomeration of free iron in the peripheral serum of patients with glaucoma and a rat model of pathological hypertension accentuated the efficacy of deferipone in impeding RGCs ferroptosis, thereby preserving visual acuity through the maintenance of iron homeostasis[31]. In a sodium iodate-induced retinal oxidative stress paradigm, the accretion of iron ions and lethal oxidative stress got identified as the catalysts for retinal pigment epithelial (RPE) ferroptosis, with the degeneration of RPE effectively palliated by HO-1 silencing or administration of the HO-1 antagonist ZnPP[32]. This inquiry endeavored to discern whether the neuroprotective attributes of Sal was affiliated with the abrogation of RGCs ferroptosis. It was ascertained that Sal enhanced the mitochondrial morphology of RGCs, as affected by *db/db* mice or HG, augmented MMP, attenuated ROS and lipid peroxidation levels, augmented SOD and GSH concentrations, reduced MDA and Fe^{2+} contents, and increased SLC7A11 and GPX4 expression levels. These observations intimate that Sal mitigated ferroptosis in RGCs, as induced by *db/db* mice or HG. Fer-1, a synthetic antioxidant and a potent and selective inhibitor of ferroptosis[33], got identified in this study to markedly diminish RGCs oxidative stress, lipid peroxidation levels, and iron aggregation when directed against HG-induced RGCs. It also potentiated the anti-ferroptosis proteins GPX4 and SLC7A11 expression, thereby inhibiting RGCs ferroptosis. These discoveries indicate that Fer-1 could mitigate cellular damage by bolstering the antioxidant potential of the System-Xc-GPX4 system, a mechanism akin to that of Sal.

HIF-1 is a transcription factor characterized by its heterodimeric structure, composed of both an α subunit and a β subunit[34]. HIF-1α, the predominant regulatory and active constituent of HIF-1, stands as one of the central regulatory molecules aiding mammalian cells in acclimating to hypoxic environments[35]. Over the temporal spectrum, a plethora of studies have elucidated the intricate involvement of HIF-1α in the orchestration of cellular ferroptosis across an array of diseases, encompassing diabetic nephropathy (DN)[36], liver fibrosis[37], and ischemic stroke[38]. Ferroptosis is posited to exacerbate DN and renal tubular damage in diabetic models, it operates *via* the mechanistic pathway involving HIF-1α/HO-1[36]. As an illustration, Sorafenib mitigates liver fibrosis by inducing ferroptosis in hepatic stellate cells through the HIF-1α/SLC7A11 pathway[37]. HO-1, an integral molecule in the cellular response to oxidative distress, principally catalyzes heme while yielding carbon monoxide, biliverdin, and free divalent iron ions[39-40]. Due to the translocation of HIF-1α to the nucleus and its role as a transcription factor, we isolated the cytoplasmic and nuclear proteins of RGC and found that HIF-1α in the nucleus under high glucose conditions increased expression, cytoplasmic HIF-1α reduced expression. Meanwhile, Sal inhibits HIF-1α translocation into the nucleus. HO-1 is a key molecule downstream of the HIF-1α signaling pathway, primarily responsible for breaking down heme to produce carbon monoxide, biliverdin, and free Fe^{2+}. When intracellular free Fe^{2+} overload occurs, it can trigger the Fenton reaction and ultimately induce cell ferroptosis[41-42]. Contemporary evidence intimates that HIF-1α overexpression directly modulates augmented HO-1 expression, thus inducing the initiation of ferroptosis[36,43]. Hence, it was hypothesized that HIF-1α could orchestrate HO-1 regulation, thereby triggering ferroptosis in RGCs cells HG induction. Ergo, the functional role and unrevealed mechanism of HIF-1α/HO-1 in HG-induced ferroptosis in RGCs cells got meticulously investigated. Subsequent to the administration of the HIF-1α inhibitor PX-478 to HG-induced RGCs cells, PX-478 appreciably elevated the expressions of GPX4 and SCL7A11 and conspicuously reduced the expression of HO-1, inferring that HIF-1α/HO-1 played a participatory role in the modulation of ferroptosis inception. In a concerted effort to further elucidate the mechanism by which Sal exerts its protective efficacy, the HIF-1α activator $CoCl_2$ got administered prior to Sal treatment. It got discerned that $CoCl_2$ nullified the anti-ferroptosis efficacy of Sal. These findings, considered in conjunction, signify that HG-induced notable upregulation of HIF-1α/HO-1 in RGCs cells may culminate in Fe^{2+} overload and cellular oxidative stress damage, inexorably leading to ferroptosis in RGCs cells.

The results of this inquiry render a pharmacological framework for the continued development of Sal as a prospective therapeutic

modality for DR. Nonetheless, several constraints inherent to this study invite scrutiny. Primarily, although Sal, as a Chinese medicinal monomer, is acknowledged to interact with multiple proteins, this investigation restricted itself to employing bioinformatics and molecular docking assays to forecast HIF-1α, which may represent the most likely target. Secondly, this research has corroborated the probable downstream transcriptional protein HO-1 of HIF-1α; however, a myriad of downstream target genes affiliated with HIF-1α remain to be meticulously explored to ascertain the precise downstream action mechanism of HIF-1α. In addition, Sal ameliorated DR *via* inhibiting RGCs apoptosis or pyroptosis, it remains to be clarified whether this is synchronous with the RGC ferroptosis in this study. Furthermore, subsequent inquiries ought to determine whether the neuroprotective impact of Sal in DR is contingent upon alternative mechanisms, such as anti-inflammatory properties. Future explorations will strive to decode other functional mechanisms of Sal and evaluate whether their inhibitory effects on RGCs ferroptosis are synchronous with other neuroprotective effects, and delineate the character of their interplay.

5. Conclusion

This inquiry authenticated the suppressive effect of Sal on ferroptosis in RGCs in DR *db/db* mice and *in vitro*. Interestingly, Sal could mitigate RGCs ferroptosis by reducing blood sugar and impeding the HIF-1α/HO-1 signaling pathway (Fig. 11). These observations not only proffer a novel perspective on the etiology of DR but also potential clinical prevention of DR and the cultivation of Sal as a therapeutic agent.

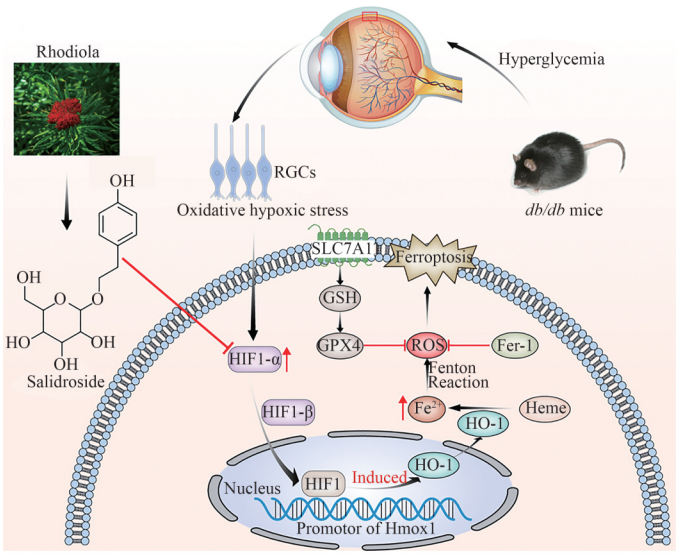

Fig. 11 This diagram illustrates how salidroside counteracts ferroptosis in RGCs of diabetic mice by interfering with the HIF-1α/HO-1 signaling pathway. Hyperglycemia can cause RGCs oxidative stress, hypoxia and other damage, these factors stimulate an increase in HIF-1α, the expression of its target gene *HO-1* is induced to increase. During the degradation of heme, HO-1 produces a large amount of Fe^{2+}, which sets off the Fenton reaction, causing the production of a significant quantity of ROS. This ROS buildup ultimately leads to ferroptosis in RGCs. Remarkably, salidroside disrupts this process by blocking the HIF-1α/HO-1 signaling pathway, effectively preventing the occurrence of ferroptosis in RGCs.

Conflict of interest

The authors declare no financial or commercial conflicts of interest.

Acknowledgements

This work was supported by the Basic Research Project for Higher Education Institutions of Liaoning Provincial Department of Education (Youth Project) (LJ212410160055); The National Natural Science Foundation of China (81571383); Foundation of Education Department of Liaoning Province of China (LJKMZ20221241); Natural Science Foundation of Liaoning Province of China (2023-MS-312).

References

[1] B. Pomeroy, A.W. Venanzi, W. Li, et al., Fluorescence angiography with dual fluorescence for the early detection and longitudinal quantitation of vascular leakage in retinopathy, Biomed. 11 (2023) 293. https://doi.org/10.3390/biomedicines11020293.

[2] Q. Xuan, Y. Ouyang, Y. Wang, et al., Multiplatform metabolomics reveals novel serum metabolite biomarkers in diabetic retinopathy subjects, Adv. Sci. 7 (2020) 2001714. https://doi.org/10.1002/advs.202001714.

[3] M. Nebbioso, A. Lambiase, M. Armentano, et al., Diabetic retinopathy, oxidative stress, and sirtuins: an in depth look in enzymatic patterns and new therapeutic horizons, Surv. Ophthalmol. 67 (2022) 168-183. https://doi.org/10.1016/j.survophthal.2021.04.003.

[4] Q. Jian, Y. Wu, F. Zhang, Metabolomics in diabetic retinopathy: from potential biomarkers to molecular basis of oxidative stress, Cells 11 (2022) 3005. https://doi.org/10.3390/cells11193005.

[5] M. Guo, Y. Zhu, Y. Shi, et al., Inhibition of ferroptosis promotes retina ganglion cell survival in experimental optic neuropathies, Redox. Biol. 58 (2022) 102541. https://doi.org/10.1016/j.redox.2022.102541.

[6] K.D. Rolev, X.S. Shu, Y. Ying, Targeted pharmacotherapy against neurodegeneration and neuroinflammation in early diabetic retinopathy, Neuropharmacology 187 (2021) 108498. https://doi.org/10.1016/j.neuropharm.2021.108498.

[7] Q. Li, Y. Cheng, S. Zhang, et al., TRPV4-induced Müller cell gliosis and TNF-α elevation-mediated retinal ganglion cell apoptosis in glaucomatous rats *via* JAK2/STAT3/NF-κB pathway, J. Neuroinflammation 18 (2021) 271. https://doi.org/10.1186/s12974-021-02315-8.

[8] H.L. Park, J.H. Kim, C.K. Park, Different contributions of autophagy to retinal ganglion cell death in the diabetic and glaucomatous retinas, Sci. Rep. 8 (2018) 13321. https://doi.org/10.1038/s41598-018-30165-7.

[9] Y.J. Chen, J.T. Chen, M.C. Tai, et al., Serum iron and risk of diabetic retinopathy, Nutrients 12 (2020) 2297. https://doi.org/10.3390/nu12082297.

[10] A. Bonet, J. Pampalona, E. Jose-Cunilleras, et al., Ferritin but not iron increases in retina upon systemic iron overload in diabetic and iron-dextran injected mice, Invest. Ophthalmol. Vis. Sci. 64 (2023) 22. https://doi.org/10.1167/iovs.64.3.22.

[11] X. Zhang, L. Xie, J. Long, et al., Salidroside: a review of its recent advances in synthetic pathways and pharmacological properties, Chem. Biol. Interact. 339 (2021) 109268. https://doi.org/10.1016/j.cbi.2020.109268.

[12] Y. Li, X. Wei, S.L. Liu,et al., Salidroside protects cardiac function in mice with diabetic cardiomyopathy *via* activation of mitochondrial biogenesis and SIRT3, Phytother. Res. 35 (2021) 4579-4591. https://doi.org/10.1002/ptr.7175.

[13] Q. Liu, Q. Luo, B. Zhong, et al., Salidroside attenuates myocardial remodeling in DOCA-salt-induced mice by inhibiting the endothelin 1 and PI3K/AKT/NFκB signaling pathways, Eur. J. Pharmacol. 962 (2023) 176236. https://doi.org/10.1016/j.ejphar.2023.176236.

[14] F. Yao, X. Jiang, L. Qiu, et al., Long-Term oral administration of salidroside alleviates diabetic retinopathy in *db/db* mice, Front. Endocrinol. 13 (2022) 861452. https://doi.org/10.3389/fendo.2022.861452.

[15] J. Li, W. Liu, Y. Wang, et al., Salidroside inhibits ganglion cell apoptosis by

suppressing the müller cell inflammatory response in diabetic retinopathy, Curr. Eye. Res. 48 (2023) 758-769. https://doi.org/10.1080/02713683.2023.2204208.

[16] L.C. Zhang, N. Li, M. Xu, et al., Salidroside protects RGC from pyroptosis in diabetes-induced retinopathy associated with NLRP3, NFEZL2 and NGKB1, revealed by network pharmacology analysis and experimental validation, Eur. J. Med. Res. 29 (2024) 60. https://doi.org/10.1186/s40001-023-01578-6.

[17] M.M. Sachdeva, Retinal neurodegeneration in diabetes: an emerging concept in diabetic retinopathy, Curr. Diab. Rep. 21 (2021) 65. https://doi.org/10.1007/s11892-021-01428-x.

[18] A. Araszkiewicz, D. Zozulinska-Ziolkiewicz, Retinal neurodegeneration in the course of diabetes-pathogenesis and clinical perspective, Curr. Neuropharmacol. 14 (2016) 805-809. https://doi.org/10.2174/1570159x14666160225154536.

[19] A.W. Qiu, D.R. Huang, B. Li, et al., IL-17A injury to retinal ganglion cells is mediated by retinal Müller cells in diabetic retinopathy, Cell. Death Dis. 12 (2021) 1057. https://doi.org/10.1038/s41419-021-04350-y.

[20] H. Jiang, H. Zhang, X. Jiang, et al., Overexpression of *D*-amino acid oxidase prevents retinal neurovascular pathologies in diabetic rats, Diabetologia 64 (2021) 693-706. https://doi.org/10.1007/s00125-020-05333-y.

[21] Y. Gong, Z.P. Chang, R.T. Ren, et al., Protective effects of adeno-associated virus mediated brain-derived neurotrophic factor expression on retinal ganglion cells in diabetic rats, Cell. Mol. Neurobiol. 32 (2012) 467-475. https://doi.org/10.1007/s10571-011-9779-x.

[22] S.B. Madrakhimov, J.Y. Yang, J.H. Kim, et al., mTOR-dependent dysregulation of autophagy contributes to the retinal ganglion cell loss in streptozotocin-induced diabetic retinopathy, Cell. Commun. Signal. 19 (2021) 29. https://doi.org/10.1186/s12964-020-00698-4.

[23] M. Jin, C. Wang, Y. Xu, et al., Pharmacological effects of salidroside on central nervous system diseases, Biomed. Pharmacother. 156 (2022) 113746. https://doi.org/10.1016/j.biopha.2022.113746.

[24] R. Hu, M. Q. Wang, S.H. Ni, et al., Salidroside ameliorates endothelial inflammation and oxidative stress by regulating the AMPK/NF-κB/NLRP3 signaling pathway in AGEs-induced HUVECs, Eur. J. Pharmacol. 867 (2020) 172797. https://doi.org/10.1016/j.ejphar.2019.172797.

[25] Y. Wang, J. Han, L. Luo, et al., Salidroside facilitates therapeutic angiogenesis in diabetic hindlimb ischemia by inhibiting ferroptosis, Biomed. Pharmacother. 159 (2023) 114245. https://doi.org/10.1016/j.biopha.2023.114245.

[26] P. Lü, Z. Zuo, W. Liu, et al., Salidroside alleviates diabetic cognitive dysfunction *via* B3galt2/F3/Contactin signaling pathway in mice, Neuroscience 512 (2023) 47-58. https://doi.org/10.1016/j.neuroscience.2022.12.008.

[27] B. Guo, Z. Zuo, X. Di, et al., Salidroside attenuates HALI *via* IL-17A-mediated ferroptosis of alveolar epithelial cells by regulating Act1-TRAF6-p38 MAPK pathway, Cell. Commun. Signal. 20 (2022) 183. https://doi.org/10.1186/s12964-022-00994-1.

[28] J. Liu, R. Kang, D. Tang, Signaling pathways and defense mechanisms of ferroptosis, FEBS. J. 289 (2022) 7038-7050. https://doi.org/10.1111/febs.16059.

[29] Q. Huang, H. Tian, L. Tian, et al., Inhibiting Rev-erbα-mediated ferroptosis alleviates susceptibility to myocardial ischemia-reperfusion injury in type 2 diabetes, Free Radic. Biol. Med. 209 (2023) 135-150. https://doi.org/10.1016/j.freeradbiomed.2023.09.034.

[30] Y. Li, Y. Wen, X. Liu, et al., Single-cell RNA sequencing reveals a landscape and targeted treatment of ferroptosis in retinal ischemia/reperfusion injury, J. Neuroinflammation 19 (2022) 261. https://doi.org/10.1186/s12974-022-02621-9.

[31] F. Yao, J. Peng, E. Zhang, et al., Pathologically high intraocular pressure disturbs normal iron homeostasis and leads to retinal ganglion cell ferroptosis in glaucoma, Cell. Death Differ. 30 (2023) 69-81. https://doi.org/10.1038/s41418-022-01046-4.

[32] Z. Tang, Y. Ju, X. Dai, et al., HO-1-mediated ferroptosis as a target for protection against retinal pigment epithelium degeneration, Redox. Biol. 43 (2021) 101971. https://doi.org/10.1016/j.redox.2021.101971.

[33] G. Miotto, M. Rossetto, M.L. Di Paolo, et al., Insight into the mechanism of ferroptosis inhibition by ferrostatin-1, Redox. Biol. 28 (2020) 101328. https://doi.org/10.1016/j.redox.2019.101328.

[34] V. Infantino, A. Santarsiero, P. Convertini, et al., Cancer cell metabolism in hypoxia: role of HIF-1 as key regulator and therapeutic target, Int. J. Mol. Sci. 22 (2021) 5703. https://doi.org/10.3390/ijms22115703.

[35] H.S. Li, Y.N. Zhou, L. Li, et al., HIF-1α protects against oxidative stress by directly targeting mitochondria, Redox. Biol. 25 (2019) 101109. https://doi.org/10.1016/j.redox.2019.101109.

[36] X. Feng, S. Wang, Z. Sun, et al., Ferroptosis enhanced diabetic renal tubular injury *via* HIF-1α/HO-1 pathway in *db/db* mice, Front. Endocrinol. 12 (2021) 626390. https://doi.org/10.3389/fendo.2021.626390.

[37] S. Yuan, C. Wei, G. Liu, et al., Sorafenib attenuates liver fibrosis by triggering hepatic stellate cell ferroptosis *via* HIF-1α/SLC7A11 pathway, Cell. Prolif. 55 (2022) e13158. https://doi.org/10.1111/cpr.13158.

[38] Y. Cui, Y. Zhang, X. Zhao, et al., ACSL4 exacerbates ischemic stroke by promoting ferroptosis-induced brain injury and neuroinflammation, Brain. Behav. Immun. 93 (2021) 312-321. https://doi.org/10.1016/j.bbi.2021.01.003.

[39] X. Li, J. Yu, L. Gong, et al., Heme oxygenase-1 (HO-1) regulates Golgi stress and attenuates endotoxin-induced acute lung injury through hypoxia inducible factor-1α (HIF-1α)/HO-1 signaling pathway, Free. Radic. Biol. Med. 165 (2021) 243-253. https://doi.org/10.1016/j.freeradbiomed.2021.01.028.

[40] H. Huang, L. Wang, F. Qian, et al., Liraglutide *via* activation of AMP-activated protein kinase-hypoxia inducible factor-1α-heme oxygenase-1 signaling promotes wound healing by preventing endothelial dysfunction in diabetic mice, Front. Physiol. 12 (2021) 660263. https://doi.org/10.3389/fphys.2021.660263.

[41] A. Loboda, M. Damulewicz, E. Pyza, et al., Role of Nrf2/HO-1 system in development, oxidative stress response and diseases: an evolutionarily conserved mechanism, Cell. Mol. Life. Sci. 73 (2016) 3221-3247. https://doi.org/10.1007/s00018-016-2223-0.

[42] S. Han, F. Lin, Y. Qi, et al., HO-1 contributes to luteolin-triggered ferroptosis in clear cell renal cell carcinoma *via* increasing the labile iron pool and promoting lipid peroxidation, Oxid. Med. Cell. Longev. 2022 (2022) 3846217. https://doi.org/10.1155/2022/3846217.

[43] Y. Wu, J. Wang, T. Zhao, et al., Di-(2-ethylhexyl) phthalate exposure leads to ferroptosis via the HIF-1α/HO-1 signaling pathway in mouse testes, J. Hazard. Mater. 426 (2022) 127807. https://doi.org/10.1016/j.jhazmat.2021.127807.